Ab initio investigation of superconductivity in orthorhombic MgPtSi

H. M. Tütüncü[a,b], Ertuğrul Karaca[a] and G. P. Srivastava[c]

[a] *Sakarya Üniversitesi, Fen-Edebiyat Fakültesi, Fizik Bölümü, 54187, Adapazarı, Turkey*

[b] *Sakarya Üniversitesi, BIMAYAM Biyomedikal, Manyetik ve Yarıiletken Malzemeler Araştırma Merkezi, 54187, Adapazarı, Turkey*

[c] *School of Physics, University of Exeter, Stocker Road, Exeter EX4 4QL, UK*

Abstract

We have performed an *ab initio* study of electronic, vibrational and superconducting properties of the orthorhombic MgPtSi by employing the density functional theory, a linear-response formalism, and the plane-wave pseudopotential method. Our electronic results suggest that the density of states at the Fermi level is primarily contributed by Pt 5d and Si 3p states with much smaller contribution from Mg electronic states. Phonon anomalies have been found for all three acoustic branches. Due to these phonon anomalies, the acoustic branches make large contributions to the average electron-phonon coupling parameter. From the Eliashberg spectral function, the value of average electron-phonon coupling parameter is found to 0.707. Using this value, the superconducting critical temperature is obtained to be 2.4 K, in excellent accordance with its experimental value of 2.5 K.

Key words: Honeycomb network; density functional theory; superconductivity; electronic structure; phonons

[1] Corresponding Author: H. M. Tütüncü Tel: +90 264 295 60 72 Fax: +90 264 295 59 50 e-Mail: tutuncu@sakarya.edu.tr

1 Introduction

Since the discovery of superconductivity in MgB_2 with a transition temperature T_c of 39.7 K [1], countless studies[1–17] of this as well as related compounds [18–32], have been carried out to establish the origin of superconductivity in them. It is well known that the high temperature superconductor MgB_2 [1] has the layered hexagonal AlB_2 type structure, where Boron atoms form a honeycomb network, consisting of graphite-like sheets separated by hexagonal layers of Mg atoms. This has attracted attention towards other compounds characterized with honeycomb network for their potential as new superconductors. Alkaline earth (AE) alumino silicides AEAlSi (AE = Ca, Sr) possess the AlB_2 structure, and exhibit superconductivity with relatively low critical transition temperatures of 7.8, and 5.1 K, respectively [18–32]. Although the critical transition temperatures of Alkaline earth alumino silicides are low, these materials contain immanent elements, and thus can be useful in application if their superconducting critical transition temperatures T_c can be improved. In addition to these silicides, β-$ThSi_2$ adopts the AlB_2-type structure and exhibits superconductivity with the T_c value of 2.41K [33]. Moreover, the ternary akaline earth metal silicide $Sr(Ga_{0.37}, Si_{0.67})_2$ also possesses the layered hexagonal AlB_2 type structure, where Si and Ga atoms are arranged in a chemically disordered honeycomb network and Sr atoms are intercalated between them. Electrical resistivity and dc magnetization measurements showed that it is a type-II superconductor with the onset temperature of 3.5 K [34]. We also mention that silicides superconductors are not only important for superconductivity, as they can be also used for Si-based electronic devices.

In 2011, superconductivity was explored for the honeycomb networked pnictide SrPtAs with the transition temperature of 2.4 K [35]. The discovery of superconductivity in this hexagonal pnictide has motivated experimentalists to study its magnetic and superconducting properties of compounds with similar layered atomic networks. Biswas and co-workers [36] have presented the magnetic and superconducting properties of locally noncentrosymmetric SrPtAs obtained by muon-spin-rotation/relaxation (μSR) measurements Recently, a ternary compound, MgPtSi, has been synthesized by solid-state reaction [37]. This material adopts the orthorhombic TiNiSi-type structure with the space group of Pnma. This material contains alternately stacked layers of Mg and PtSi honeycomb network, which is reminiscent of MgB_2, and the buckling of the honeycomb network leads to an orthorhombic distortion. Electrical and magnetic studies [37] revealed that MgPtSi is a superconductor with a critical transition temperature of 2.5 K. Kudo and coworkers [37] have studied the electronic properties of MgPtSi using the density-functional theory. An examination of their results shows a strong Pt-5d character at the Fermi level.

Although the electronic properties of MgPtSi have been studied, no experimental or theoretical efforts have been made to calculate its phonon dispersion relations and phonon density of states, both of which are considered to play an important role in determining BCS-type superconductivity. With this in mind we have aimed at making *ab initio* calculations of the electronic and phonon properties of MgPtSi. The

electronic calculations are carried out using the plane wave pseudopotential method within the generalized gradient approximation of the density functional scheme. This is followed by the application of a linear response scheme [38–40] in order to investigate its dynamical properties. Then, the linear response method and the Migdal-Eliashberg approach [38–43] have been employed to determine the Eliashberg spectral function. By integrating the Eliashberg spectral function, the average electron-phonon coupling parameter is calculated. Using the calculated value of average electron-phonon coupling parameter, the superconducting transition temperature T_c is obtained and compared with the recently measured experimental value [37].

2 Computational Details

MgPtSi adopts the orthorhombic TiNiSi-type of crystal structure, with space group, no. 62, Pnma, and four formula units per primitive cell [37]. The atomic configuration contains four Mg atoms at the (4c) (x_{Mg}, 1/4, z_{Mg}) position, four Pt atoms at the 4(c) (x_{Pt}, 1/4, z_{Pt}) position and four Si atoms at the 4(c)(x_{Si}, 1/4, z_{Si}) position. Thus, this orthorhombic structure is described by three lattice parameters (a, b and c) and six internal parameters (x_{Mg}, z_{Mg}, x_{Pt}, z_{Pt}, x_{Si} and z_{Si}). The six internal parameters are determined by the total energy minimization procedure using the QUANTUM ESPRESSO code [40], which uses a plane-wave basis set of the expansion of the Kohn-Sham orbitals [44]. While we have optimized these internal parameters optimizing the three lattice parameters (a, b, c) is not a straight forward procedure, and it is possible to find different combinations of these leading to similarly low-energy configuration. For this reason, the experimental lattice parameters [37], $a = 6.5324$ $\mathring{A}$, $b = 4.1005$ $\mathring{A}$ and $c = 7.1752$ $\mathring{A}$ are taken as input data in our *ab initio* calculations. A similar procedure has been adopted by several other research groups which studying similar systems, see e.g. Refs. [45–49]. We also mention here that due to crystal transnational and point group symmetries, there will be no imaginary phonon frequencies when using the experimental lattice constants. The electronic exchange-correlation terms are included within the Perdew-Burke-Ernzerhof method under the generalized gradient approximation (GGA) [50]. Ion-electron interactions were treated by using the norm-conserving pseudopotentials [51,52]. The wave functions are expanded in a plane wave basis set with the kinetic energy cutoff of 60 Ry. Self-consistent solutions of the Kohn-Sham equations [44] are achieved by employing a set of Monkhorst-Pack special $\boldsymbol{k}$ points [53] within the irreducible part of the Brillouin zone. The numerical integration of the Brillouin zone for the total-energy calculations is made by using a 6×6×6 Monkhorst-Pack $\boldsymbol{k}$-point sampling [53]. On the other hand, the electronic structure and the electronic density of states have been determined with a (24×24×24) grid.

The density functional perturbation theory (DFPT) [38–40], based on a linear response scheme, which is one of the most well-liked methods of lattice dynamics, is utilized to investigate the vibrational properties of this compound. The Monkhorst-Pack $6 \times 6 \times 6$ $\boldsymbol{k}$-points grid within an irreducible part of the Brillouin zone is

chosen for phonon calculations. We have calculated eight dynamical matrices which are Fourier transformed to achieve the full phonon spectrum and the vibrational density of states.

Using the first-principles results for phonons, the Migdal-Eliashberg approach [38,41–43] was employed for determining superconducting properties of solids. A denser 24×24×24 $\boldsymbol{k}$-points grid is used for an accurate evaluation of the electron-phonon interaction matrix element, which is expressed as [38]

$$g^{\boldsymbol{q}j}_{(\boldsymbol{k}+\boldsymbol{q}),m;\boldsymbol{k}n} = \sqrt{\frac{\hbar}{2M\omega_{\boldsymbol{q}j}}} \left\langle \phi_{(\boldsymbol{k}+\boldsymbol{q})m} | \boldsymbol{e}_{\boldsymbol{q}j} \cdot \vec{\nabla} V^{SCF}(\boldsymbol{q}) | \phi_{\boldsymbol{k}n} \right\rangle , \tag{1}$$

where M shows atomic mass and $\vec{\nabla} V^{SCF}(\boldsymbol{q})$ is the derivative of the self-consistent effective potential with respect to the atomic displacement caused by a phonon with wave vector $\boldsymbol{q}$. the Eliashberg spectral function measures the effectiveness of phonons with energy ω to scatter electrons from one part of the Fermi surface to another part. This function can be given as [38,39];

$$\alpha^2 F(\omega) = \frac{1}{2\pi N(E_F)} \sum_{\boldsymbol{q}j} \frac{\gamma_{\mathbf{q}j}}{\hbar\omega_{\boldsymbol{q}j}} \delta\left(\omega - \omega_{\boldsymbol{q}j}\right), \tag{2}$$

$$\gamma_{\boldsymbol{q}j} = 2\pi\omega_{\boldsymbol{q}j} \sum_{\boldsymbol{k}nm} |g^{\boldsymbol{q}j}_{(\boldsymbol{k}+\boldsymbol{q})m;\boldsymbol{k}n}|^2 \delta(\varepsilon_{\boldsymbol{k}n} - \varepsilon_F) \delta(\varepsilon_{(\boldsymbol{k}+\boldsymbol{q})m} - \varepsilon_F), \tag{3}$$

where $N(E_F)$ shows the electronic density of states at the Fermi level and $\gamma_{\boldsymbol{q}j}$ is known as the phonon line-width. The frequency dependent electron-phonon coupling parameter $\lambda(\omega)$, and the frequency accumulative electron-phonon coupling parameter $\lambda_{\mathrm{acc}}(\omega)$ can be presented as

$$\lambda(\omega) = 2\frac{\alpha^2 F(\omega)}{\omega}, \tag{4}$$

$$\lambda_{\mathrm{acc}}(\omega) = \int_0^{\omega} \lambda(\omega') d\omega'. \tag{5}$$

The Allen-Dynes modification of the McMillian can be used to calculate the superconducting transition temperature (T_c). This formula can be expressed as [43]

$$T_C = \frac{\omega_{\ln}}{1.2} \exp\left(-\frac{1.04(1+\lambda)}{\lambda - \mu^*(1+0.62\lambda)}\right), \tag{6}$$

$$\omega_{\ln} = \exp\left(\frac{1}{\lambda}\sum_{\boldsymbol{q}j} \lambda_{\boldsymbol{q}j} \ln\omega_{\boldsymbol{q}j}\right). \tag{7}$$

where $\omega_{\ln}$ is known as the logarithmically averaged frequency. The values of the Coulomb pseudo-potential (μ^*) changes between 0.10 and 0.16 [43]. In our calculations, the average of these values (μ^*=0.13) are used.

3 Results

3.1 Structural and Electronic Properties

From our *ab initio* calculations, the positions of the atoms in a unit cell for MgPtSi with the TiNiSi-type crystal structure are found to be: Mg (0.005, 0.250, 0.684), Pt (0.183, 0.250, 0.069) and Si (0.3013, 0.250, 0.387). These values can be compared with the corresponding experimental values [37]: Mg (-0.020, 0.250, 0.693), Pt (0.179, 0.25 0.066) and Si (0.289, 0.250, 0.361). The crystal structure, with the relaxed atomic positions, is shown in Fig. 1. As can be seen from the $y-z$ projection of this structure (see Fig. 1(b), Pt and Si alternately fill sites in the honeycomb network while Mg is placed between two Pt-Si honeycomb layers. The arrangement of the Pt-Si six-membered ring is of the 'chair' type, as is also found for the Ni-Si network in MnNiSi structure [54], in which the relative heights of the Pt and Si atoms in neighbouring arms of the ring are in opposite directions. This is in agreement with the work of Kudo *et al* [37]. As can be seen from the $x-z$ projection of this structure (see Fig. 1(c), the buckling of adjacent PtSi layers is in opposite directions along the x axis, resulting in the generation of interlayer chemical bonds between Pt and Si along this axis. The closest Pt-Si separations within the honeycomb layers are found to be 2.405 $\mathring{A}$ and 2.436 $\mathring{A}$ which can be compared with their experimental values [37] of 2.241 $\mathring{A}$ and 2.529 $\mathring{A}$. Furthermore, the closest Pt-Si separation between the adjacent honeycomb layers found to be 2.509 $\mathring{A}$ is somewhat shorter than its experimental value [37] of 2.597 $\mathring{A}$. In this crystal structure, the Mg layers function as the so-called charge reservoir layers, which provide electron transfer from the Mg layers to the [PtSi] layers. Thus, the neighboring layers Mg-[PtSi] are coupled due to ionic interactions. But in the PtSi layers, there are covalent bonds between Pt and Si atoms with some metallic character. Thus, the bonding in the the TiNiSi-type crystal structure of MgPtSi can be classified as a mixture of covalent, metallic and ionic.

Fig. 2 (a) shows the calculated electronic energy band structure for MgPtSi along the high symmetry directions in the simple orthorhombic Brillouin zone (BZ). The overall band profile is found to be in good agreement with previous theoretical results [37]. The valence and conduction bands considerably overlap indicating the metallic nature of this material. The lowest four bands mainly come from the s electrons of Si atoms. These 's' bands are well separated by a gap of 1.5 eV from the main valence band region from -7.1 eV to the Fermi level. The total density of states (DOS) and the partial DOS of each element, broken up into site and angular momentum contributions, are shown in Fig. 2 (b). As mentioned before the Si 3s part extends from -11.6 to -8.6 eV with some contributions from the Mg 3p and Pt electronic states. For energy window from -7.1 to -6.0 eV, there is high degree of hybridization of Pt 5d states with Si 3p states, which is the evidence of a covalent interaction between Pt and Si atoms. For energy window from -6.0 to -2.3 eV, the DOS features are mainly characterized by Pt 5d orbitals with lesser contribution from Si and Mg 3p orbitals. Finally, Si 3p, Pt 5d, Pt 6p and Mg 3p orbitals are

present in the energy intervals from -3 to 0 eV. Consequently, we can state that the partial DOS of Pt and Si are widely distributed below the Fermi level whereas the contribution from the Mg state is relatively small. This result is expected because Mg atoms are nearly in the form of cations Mg^{2+} and behave like electronic donors.

It is important to identify the origin of the density of states at the Fermi level, which is essential for governing superconducting properties because Cooper pairs in the BCS theory can be formed by electrons which have energies close to the Fermi level. The value of density of states at the Fermi level ($N(E_F)$) is composed of approximately 10% from Mg electronic states ($N(E_F^{Mg}) = 0.353$ states/eV), 47% from Pt electronic states ($N(E_F^{Pt}) = 1.6591$ states/eV) and 43% Si electronic states ($N(E_F^{Si}) = 1.5179$ states/eV). In particular, Si 3p and Pt 5d states alone contribute to $N(E_F)$ up to 37% and 27% respectively. Thus, we can emphasize that Si 3p and Pt 5d electrons are most efficient in developing the superconducting properties of MgPtSi. Our calculated value of $N(E_F)$ is larger than a previous theoretical value of 3.10 States/eV [37]. There are two possible reasons for this difference. Firstly, the authors of Ref. [37] used the WIEN2K package for electronic calculations, but did not spell out their choice of the exchange-correlation functional. Secondly, these authors used the experimental lattice constants and the atomic positions within the unit cell for their electronic calculations. As we have already mentioned, there are subtle differences between out optimised internal coordinates and the experimentally refined structural parameters in Ref. [37]. In particular, our calculated interlayer Pt-Si distance (2.509 Å) is somewhat shorter than the experimental value of 2.597 Å. Such small differences may also cause some differences in the estimate for the density of states at the Fermi level ($N(E_F)$). Our calculated total electronic density of states at the Fermi level $N(E_F) = 3.53$ states/eV has contributions from Si 3p and Pd 5d orbitals of approximately 27% and 37%, respectively. Further LDA+U calculations produce $N(E_F) = 3.40$ states/eV, of which contributions from Si 3p and Pd 5d orbitals are 26% and 40%, respectively. Thus we conclude that the main reason for the is due to the difference the internal structural parameters.

3.2 Electron-phonon interaction

We first analyze the zone-center phonon modes of MgPtSi categorized by the irreducible representations of the point group D_{2h}(mmm). As given by group theory, the symmetries of the zone-center optical phonon modes are given as:

$$\Gamma = 6A_g + 3B_{3g} + 3A_u + 3B_{1g} + 5B_{1u} + 6B_{2g} + 5B_{3u} + 2B_{2u}$$

where the suffixes g and u describe the even and odd parities. The frequencies (ν) and electron-phonon coupling parameters (λ) of the zone-center optical phonon modes are given in Tab. 1. The largest contributions to the electron-phonon coupling parameter λ come from the two lowest A_g phonon modes. Their contributions are $\lambda(A_g(\nu = 1.408 \text{ THz})) = 0.363$ and $\lambda(A_g(\nu = 2.611 \text{ THz})) = 0.1691$. As shown in Fig. 3, these optical modes result from the two Pt-Si chains in each unit cell vibrating against each other along the z axis. The large values of λ for these modes

can be explained: the density of states at the Fermi level is mainly dominated by the Pt d and Si p states and the Pt-Si chain vibrations facilitate the overlap of the Pt and Si electronic states. The large contribution to the electron-phonon interaction from these A_g phonon modes can also be explained by using the McMillan-Hopfield expression $\lambda = \frac{N(E_F)<I^2>}{M<\omega^2>}$, where $< I^2 >$ is the averaged square of the electron-phonon matrix, $< \omega^2 >$ is the averaged square of the phonon frequency, and M is the mass involved. This expression clearly indicates that a combination of softer phonon mode and a larger $N(E_F)$ leads to a large electron-phonon coupling parameter.

A trustworthy calculation of electron-phonon coupling needs knowledge of the full phonon dispersion relations throughout the Brillouin zone. Fig. 4 (a) displays the phonon dispersion curves along high symmetry lines in the simple orthorhombic Brillouin zone. Since the primitive unit cell contains twelve atoms, 36 phonon modes exist in the phonon dispersion curves of MgPtSi. Absorbing features are observed in this phonon spectrum. First, no imaginary phonon frequency exist at any symmetry direction which indicates that MgPtSi is dynamically stable in the orthorhombic TiNiSi-type structure. Secondly, the stabilized phonon modes can be divided into four parts with visible gaps of 0.9, 0.2 and 0.6 THz due to the mass difference between different type of elements. Thirdly, all phonon bands are dispersive along the high symmetry directions. Finally, there is strong overlap between low-frequency optical phonon spectrum and the acoustic phonon spectrum. This strong interaction may cause the heat carrying acoustic branches being scattered by low-frequency optical branches and reduce the thermal conductivity of MgPtSi. To understand the contributions of various phonon modes in the phonon spectrum, the results of total and partial density of vibrational states for this material are illustrated in Fig. 4 (b). The Pt-related phonons located at low-frequency region are mainly confined to the frequency region below 3.7 THz. They contribute predominantly to the acoustic phonon branches and low-frequency optical branches. However, Pt vibrations almost vanish above 3.7 THz due to the heaviest mass of Pt. The Si-related and Mg-related phonon densities are quite dispersive, partaking in lattice vibrations over a whole range of phonon frequencies due to their smaller masses as compared to the mass of Pt atom. In particular, considerable Pt-Si hybridization is found below 1.5 THz. Smaller Mg contribution is observed in this low-frequency region. Finally, the Mg atoms dominate in the frequency region from 4.6 to 7.9 THz while Si atoms dominate in the frequency region above 8 THz.

The most interesting feature of the phonon dispersion relations for MgPtSi is the anomalous dispersion shown by the lower transverse acoustic branch (TA_1), the upper transverse acoustic branch (TA_2) and the longitudinal branch (LA). The phonon anomalies of the acoustic branches may be crucial for superconductivity in MgPtSi since previous theoretical studies on the $LuNi_2B_2C$ type superconductors [55] have confirmed that phonon anomalies lead to strong electron-phonon interaction. In order to find out the positive relation between the noted phonon anomalies and the electron-phonon interaction, we illustrate the frequency-dependent electron-phonon coupling parameters of the acoustic phonon branches along the S-Γ-Z direction in Fig. 5 (a). The first interesting feature is the softening of TA_2 branch along the Γ-S direction. Thus, the TA_2 branch has lower frequency than that of TA_1 branch in the

large part of Γ-S direction. Due to this phonon anomaly, the electron-phonon coupling parameter of the TA_2 branch approaches its largest value of 0.563 at $\mathbf{q}=\frac{2\pi}{a}(0.25, 0.25\frac{a}{b}, 0.000)$. Along the Γ-S direction, the phonon anomaly has been also observed for the LA branch. Thus, the electron-phonon coupling parameter of this phonon modes has its peak value of 0.339 at $\mathbf{q}=\frac{2\pi}{a}(0.25, 0.125\frac{a}{b}, 0.000)$. Furthermore, phonon anomalies for the acoustic modes are also found along the Γ-R-T-Γ direction. We show the frequency-dependent electron-phonon coupling parameters of the acoustic phonon branches along the Γ-R-T-Γ direction in Fig. 5 (b). We have to mention that transverse acoustic branches are doubly degenerate along the R-T direction. The most notable feature of this figure is that the electron-coupling parameters of TA_1 and TA_2 branches hardens rapidly along the Γ-T direction due to the striking phonon anomalies of these acoustic branches. At the T point, the electron-phonon coupling parameters of these phonon branches become degenerate with the value of 1.138. We are thus able to conclude that the acoustic phonon branches are more involved in the process of scattering of electrons than the optical phonon branches.

The main destination of the present work is to analyze the strength of the electron-phonon interaction in MgPtSi in order to clearly understand the existence of superconductivity in this material. To this end, Fig. 6 shows the Eliashberg spectral function $\alpha^2F(\omega)$ and the frequency accumulative electron-phonon coupling parameter $\lambda_{\rm acc}(\omega)$. As can be seen from this figure, the value of the accumulative electron-phonon coupling parameter $\lambda_{\rm acc}(\omega)$ increases linearly with rise in frequency in the region below 1.5 THz. The calculated contribution for $\lambda_{\rm acc}$ from this frequency region is 52%. This large contribution is expected because the phonon modes in this frequency region arise from the coupled motion of Pt and Si atoms. Furthermore, the density of states at the Fermi level is mainly dominated by Pt and Si electronic states. The calculated contribution for $\lambda_{\rm acc}$ from the frequency region between 1.5 and 3.7 THz is 31%. Phonon modes in this frequency region are dominated by the vibrations Pt atoms. This is not surprising because the electronic states of Pt atoms make the largest contribution to the total density of states at the Fermi level. The accumulative electron-phonon coupling parameter $\lambda_{\rm acc}(\omega)$ increases like a small step function in the frequency region between 4.6 and 7.9 THz. This results is also expected because phonon modes in this frequency region arise from the vibrations of Mg atoms which make the smallest contribution to the density of states at the Fermi level. The calculated contribution for $\lambda_{\rm acc}$ from this frequency region is 6%. Phonon modes above 8.1 THz make a small contribution of 11% to $\lambda_{\rm acc}$. This small contribution can be easily understood by noting that higher frequency phonons make the factor $\frac{1}{\omega}$ smaller in producing $\lambda_{\rm acc}(\omega)$ (see Eqs. (4,5)). With Eq. 6, the value of the average electron-phonon coupling parameter λ is found to be 0.707, a value indicative of medium strength. Using Eq. 7, the value of ω_{ln} is calculated to be 86.53 K. Finally, the superconducting transition temperature T_c is found to be 2.4 K when taking the value of μ^* to be 0.13 (which lies in the typical range of μ^* values). The calculated value of T_c is in excellent agreement with its experimental value of 2.5 K [37]. At the end, using the Allen-Dynes formula and taking typical values of $\mu^* =$ 0.10, 0.11, 0.12, 0.13, 0.14, 0.15 and 0.16, we find T_c= 3.1, 2.8, 2.6, 2.4, 2.2, 2.0 and 1.7 K, respectively. The average of these values is again found to be 2.4 K which compares very well with its experimental value of 2.5 K [37].

3.3 Summary

In this work, we have studied the electronic, vibrational, and superconducting properties of MgPtSi crystallizing in the orthorhombic TiNiSi-type of crystal structure applying density functional theory within a generalised gradient approximation. The overall band profile of this material is found to be in good accordance with previous theoretical results. The bonding in this material can be classified as a mixture of metallic,ionic and covalent contributions. From the analysis of the total and partial electronic density of states, we have found that the states around the Fermi level are mainly dominated by Pt and Si electronic states with much smaller contribution coming Mg electronic states. This results confirms the active roles of Pt and Si atoms in determining the electronic and superconducting properties of MgPtSi. In addition to the electronic properties, lattice dynamics of MgPtSi has been investigated by employing a linear response approach based on density functional perturbation theory. Our phonon results indicate that MgPtSi is dynamically stable in the orthorhombic TiNiSi-type structure, as no instabilities in the phonon dispersion curves have been found. The calculated total and partial phonon density of states for MgPtSi show that the low-frequency region below 3.7 THz are mainly dominated by the vibrations of Pt atoms while the Si-related and Mg-related phonon densities are very dispersive, partaking in lattice vibrations over a whole range phonon frequencies due to their smaller masses as compared to the mass of Pt atom. However, the most impressive features in the phonon dispersion relations for MgPtSi are the phonon anomalies in the acoustic phonon branches. We have shown that these phonon anomalies are crucial for superconductivity in MgPtSi because they produce the largest contribution to the electron-phonon interaction in this material.

The phonon spectrum and the electron-phonon matrix elements are used to calculated the Eliashberg function from which the superconducting properties can be determined. A detailed examination of the Eliashberg function indicates that the phonon modes below 1.5 THz are significantly more involved in the process of scattering of electrons than the phonon modes with higher frequencies. This result is expected because these phonon modes are characterized by the coupled motion of Pt and Si atoms which make large contributions to the density of states at the Fermi level ($N(E_F)$). From the integration of Eliashberg spectral function, the value of the average electron-phonon coupling parameter is determined to be 0.707. Thus, we conclude that electron-phonon interaction in MgPtSi is of medium strength. Finally, using the Allen-Dynes modified McMillian equation with the screened Coulomb pseudopotential parameter $\mu^* = 0.13$, the value of the superconducting critical temperature (T_c) is determined to 2.4 K which compares very well with its experimental value of 2.5 K.

ACKNOWLEDGEMENT

The calculations were performed using the Intel Nehalem (i7) cluster (ceres) at the University of Exeter.

References

[1] J. Nagamatsu, N. Nakagawa, T. Muranaka, Y. Zenitani, and J. Akimitsu, Nature 410 (2001) 63-64 .

[2] A. Sharoni, I. Felner, and O. Millo, Phys. Rev. B 63 (2001) 220508(R)/1-4.

[3] J. D. Jorgensen, D. G. Hinks, and S. Short, Phys. Rev. B 63 (2001) 224522/1-5.

[4] T. Takahashi, T. Sato, S. Souma, T. Muranaka, and J. Akimitsu, Phys. Rev. Lett. 86 (2001) 4915-4917.

[5] H. Kusunose, T. M. Rice, and M. Sigrist, Phys. Rev. B 66 (2002) 214503/1-5.

[6] L. Lyard, P. Samuely, P. Szabo, T. Klein, C. Marcenat, L. Paulius, K. H. P. Kim, C. U. Jung, H.-S. Lee, B. Kang, S. Choi, S.-I. Lee, J. Marcus, S. Blanchard, A. G. M. Jansen, U. Welp, G. Karapetrov, and W. K. Kwok, Phys. Rev. B 66 (2002) 180502(R)/1-4.

[7] Yu. Eltsev, K. Nakao, S. Lee, T. Masui, N. Chikumoto, S. Tajima, N. Koshizuka, and M. Murakami Phys. Rev. B 66 (2002) 180504(R)/1-4.

[8] G. Profeta, A. Continenza, F. Bernardini, and S. Massidda Phys. Rev. B 66 (2002) 184517/1-7.

[9] C. U. Jung, J. Y. Kim, P. Chowdhury, Kijoon H. P. Kim, Sung-Ik Lee, D. S. Koh, N. Tamura, W. A. Caldwell, and J. R. Patel Phys. Rev. B 66 (2002) 184519/1-5.

[10] T. Masuda, K. Uchinokura, T. Hayashi, and N. Miura, Phys. Rev. B 66 (2002) 174416/1-7.

[11] S. V. Barabash and D. Stroud, Phys. Rev. B 66 (2002) 172501/1-4.

[12] N. Jiang, B. Jiang, J. C. H. Spence, R. C. Yu, S. C. Li, and C. Q. Jin Phys. Rev. B 66 (2002) 172502/1-4.

[13] G. Papavassiliou, M. Pissas, M. Karayanni, M. Fardis, S. Koutandos, and K. Prassides Phys. Rev. B 66 (2002) 140514(R)/1-4.

[14] K. Kokko, V. Kulmala, and J. A. Leiro, Phys. Rev. B 66 (2002) 165114/1-4.

[15] V. A. Ivanov, M. A. Smondyrev, and J. T. Devreese, Phys. Rev. B 66 (2002) 134519/1-6.

[16] T. Park, M. B. Salamon, C. U. Jung, Min-Seok Park, K. Kim, and Sung-Ik Lee Phys. Rev. B 66 (2002) 134515/1-5.

[17] A. V. Sologubenko, J. Jun, S. M. Kazakov, J. Karpinski, and H. R. Ott, Phys. Rev. B 66 (2002) 014504/1-8.

[18] B. Lorenz, J. Lenzi, J. Cmaidalka, R.L Meng, Y.Y Sun, Y.Y Xue, C.W ChuP, Physica C 383 (2002) 191-196.

[19] A. K. Ghosh, M. Tokunaga, and T. Tamegai Phys. Rev. B 68 (2003) 054507/1-5.

[20] B. Lorenz, J. Cmaidalka, R. L. Meng, and C. W. Chu Phys. Rev. B 68 (2003) 014512/1-6.

[21] I. I. Mazin and D. A. Papaconstantopoulos Phys. Rev. B 69 (2004) 180512(R)/1-4.

[22] T. Tamegai, K. Uozato, S. Kasahara, T. Nakagawa, M. Tokunaga, Physica C 208 (2005) 426431.

[23] S. Kuroiwa, H. Sagayama, T. Kakiuchi, H. Sawa, Y. Noda, and J. Akimitsu Phys. Rev. B 74 (2006) 014517/1-5.

[24] R. Prozorov, T. A. Olheiser, R. W. Giannetta, K. Uozato, and T. Tamegai Phys. Rev. B 73 (2006) 184523/1-4.

[25] H. Sagayama, Y. Wakabayashi, H. Sawa, T. Kamiyama, A. Hoshikawa, S. Harjo, K. Uozato, A. K. Ghosh, M. Tokunaga, and T. Tamegai, J. Phys. Soc. Jpn. 75 (2006) 043713/1-4.

[26] S. Kuroiwa, T. Takasaki, T. Ekino, and J. Akimitsu Phys. Rev. B 76 (2007) 104508/1-5.

[27] S. Kuroiwa, A. Nakashima, S. Miyahara, N. Furukawa, and J. Akimitsu, J. Phys. Soc. Jpn. 76 (2007) 113705/1-4.

[28] S. Kuroiwa, A. Q. R. Baron, T. Muranaka, R. Heid, K.-P. Bohnen, and J. Akimitsu Phys. Rev. B 77 (2008) 140503(R)/1-4.

[29] S. Kuroiwa, T. Hasegawa, T. Kondo, N. Ogita, M. Udagawa, and J. Akimitsu Phys. Rev. B 78 (2008) 184303/1-10.

[30] L. Boeri, J. S. Kim, M. Giantomassi, F. S. Razavi, S. Kuroiwa, J. Akimitsu, and R. K. Kremer Phys. Rev. B 77 (2008) 144502/1-7.

[31] S. Lupi, L. Baldassarre, M. Ortolani, C. Mirri, U. Schade, R. Sopracase, T. Tamegai, R. Fittipaldi, A. Vecchione, and P. Calvani, Phys. Rev. B 77 (2008) 054510/1-5.

[32] R. Ma, G.Q. Huang, W. Wang, H.B. Shu, S. Liu, M. Liu, Physica C 468 (2008) 2233-2240.

[33] G. F. Hardy and J. K. Hulm, Phys. Rev. 93 (1954) 1004-1016.

[34] M. Imai, E. Abe, J. Ye, K. Nishida, T. Kimura, K. Honma, H. Abe, and H. Kitazawa, Phys. Rev. Lett. 87 (2001) 077003/1-4.

[35] Y. Nishikubo, K. Kudo and M. Nohara, J. Phys. Soc. Jpn., 80 (2011) p.055002/1-2.

[36] P. K. Biswas, H. Luetkens, T. Neupert, T. Strzer, C. Baines, G. Pascua, A. P. Schnyder, M. H. Fischer, J. Goryo, M. R. Lees, H. Maeter, F. Brckner, H.-H. Klauss, M. Nicklas, P. J. Baker, A. D. Hillier, M. Sigrist, A. Amato, and D. Johrendt, Phys. Rev. B 87 (2013) 180503/1-5.

[37] K. Kudo, K. Fujimura, S. Onari, H. Ota, and M. Nohara Phys. Rev. B 91 (2015) 174514/1-5.

[38] R. Bauer, A. Schmid, P. Pavone, and D. Strauch Phys. Rev. B 57 (1998) 11276/1-7.

[39] S. Baroni, S. de Gironcoli, A. Dal Corso, and P. Giannozzi Rev. Mod. Phys. 73 (2001) 515-562.

[40] P. Giannozzi, S. Baroni, N. Bonini, M. Calandra, R. Car, C. Cavazzoni, D. Ceresoli, G. L. Chiarotti, M. Cococcioni, I. Dabo, A.D. Corso, S. de Gironcoli, S. Fabris, G. Fratesi, R. Gebauer, U. Gerstmann, C. Gougoussis, A. Kokalj, M. Lazzeri, L. Martin-Samos, N. Marzari, F. Mauri, R. Mazzarello, S. Paolini, A. Pasquarello, L. Paulatto, C. Sbraccia, S. Scandolo, G. Sclauzero, A.P. Seitsonen, A. Smogunov, P. Umari and R.M. Wentzcovitch, J. Phys.: Condens. Matter 21 (2009) p.395502/1-19.

[41] A. B. Migdal, Zh. Eksp. Teor. Fiz. 34 (1958) 1438.

[42] G. M. Eliashberg, Sov. Phys. JETP. 11 (1960) 696-703.

[43] P. B. Allen and R. C. Dynes, Phys. Rev. B 12 (1975) 905-922.

[44] W. Kohn and L. J. Sham, Phys. Rev. 140 (1965) A1133-A1138.

[45] A. Subedi and D. J. Singh, Phys. Rev. B 80 (2009) 092506/1-4.

[46] D. Reznik, K. Lokshin, D. C. Mitchell, D. Parshall, W. Dmowski, D. Lamago, R. Heid, K.-P. Bohnen, A. S. Sefat, M. A. McGuire, B. C. Sales, D. G. Mandrus, A. Subedi, D. J. Singh, A. Alatas, M. H. Upton, A. H. Said, A. Cunsolo, Yu. Shvydko, and T. Egami, Phys. Rev. B 80 (2009) 214534/1-5.

[47] H. M. Tütüncü and G. P. Srivastava, Appl. Phys. Lett. 104 (2014) 022603/1-5.

[48] D. J. Singh, Phys. Rev. B 91 (2015) 214420/1-4.

[49] D. J. Singh, Phys. Rev. B 92 (2015) 174403/1-5.

[50] J. P. Perdew, K. Burke, and M. Ernzerhof, Phys. Rev. Lett. 77 (1996) 3865-3868.

[51] S. Goedecker, M. Teter, and J. Hutter, Phys. Rev. B 54 (1996) 1703-1710.

[52] C. Hartwigsen, S. Goedecker, and J. Hutter, Phys. Rev. B 58 (1998) 3641-3662.

[53] H. J. Monkhorst and J. D. Pack, Phys. Rev. B 13 (1976) 5188-5192.

[54] G. A. Landrum, R. Hoffmann, J. Evers and H. Boysen, Inorg. Chem. 37 (1998) 5754.

[55] H. M. Tütüncü, H. Y. Uzunok, Ertuğrul Karaca, G. P. Srivastava, S. Özer, and Ş. Uğur Phys. Rev. B 92 (2015) 054510/1-17.

Table 1
Calculated zone-center phonon modes (ν in THz) and their electron-phonon coupling parameters(λ) for the orthorhombic MgPtSi.

Mode	ν	λ	Eigen Characters	Mode	ν	λ	Eigen Characters
A_g	1.408	0.363	Pt+Si+Mg	B_{3g}	1.632	0.085	Pt+Si+Mg
A_u	2.061	0.004	Pt+Si+Mg	B_{1g}	2.302	0.032	Pt+Si+Mg
B_{1u}	2.558	0.013	Pt+Si+Mg	A_g	2.611	0.169	Pt+Si
B_{2g}	3.122	0.029	Pt+Si+Mg	B_{2g}	3.510	0.018	Pt+Mg
B_{3u}	3.682	0.012	Pt+Mg	B_{3u}	4.738	0.004	Mg+Si
B_{1u}	4.968	0.001	Mg+Si	A_g	5.455	0.015	Mg+Si
B_{2u}	5.509	0.001	Mg+Si	B_{1g}	5.769	0.002	Mg+Si
B_{2g}	5.991	0.004	Mg+Si	A_u	5.992	0.000	Mg
A_g	6.058	0.016	Mg+Si	B_{3u}	6.275	0.001	Mg+Si
B_{3g}	6.577	0.005	Mg	B_{1u}	7.512	0.001	Mg+Si
B_{2g}	7.800	0.015	Mg+Si	B_{1u}	8.346	0.009	Si+Mg
B_{2g}	8.603	0.008	Si+Mg	B_{3u}	8.696	0.004	Si+Mg
A_g	9.172	0.018	Mg+Si	A_u	9.938	0.001	Si
B_{3g}	10.108	0.001	Si	B_{1u}	10.115	0.004	Si+Mg
B_{2u}	10.279	0.003	Si+Mg	A_g	10.315	0.028	Si
B_{3u}	10.642	0.005	Si	B_{1g}	10.838	0.003	Si+Mg
B_{2g}	11.310	0.023	Si+Mg				

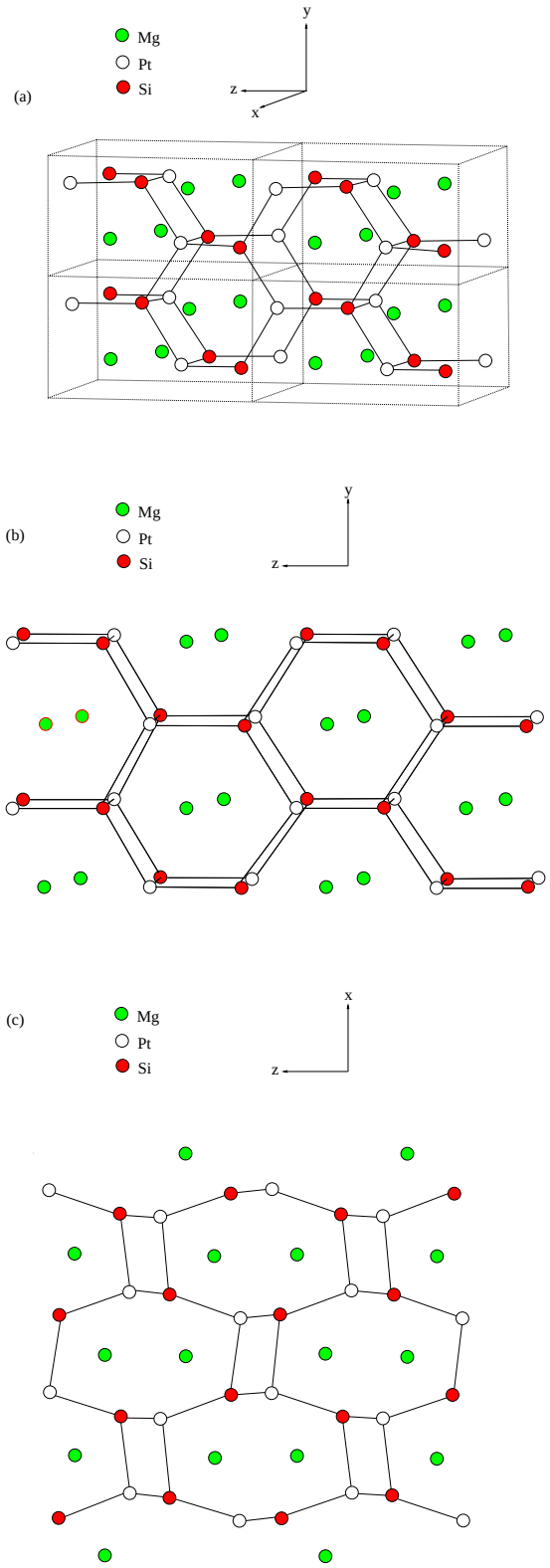

Fig. 1. The TiNiSi-type crystal structure of MgPtSi viewed in the (a) three dimensiondal, (b) y-z plane and (c) x-z plane.

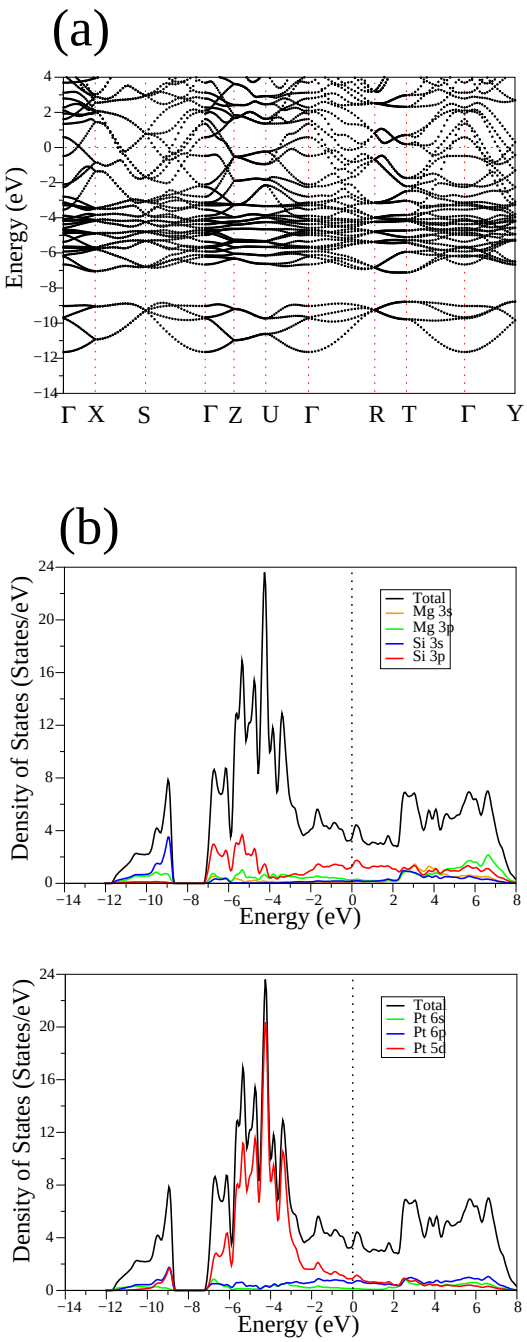

Fig. 2. The electronic band structure and density of states for MgPtSi. The Fermi level is fixed at 0 eV. The high-symmetry points in the Brillouin zone in cartesian coordinates are: Γ= $\frac{2\pi}{a}$(0.00, 0.00, 0.00), X = $\frac{2\pi}{a}$(0.50, 0.00, 0.00), S = $\frac{2\pi}{a}$(0.50, $\frac{a}{2b}$, 0.00), Z= $\frac{2\pi}{a}$(0.00, 0.00, $\frac{a}{2c}$), U = $\frac{2\pi}{a}$(0.50, 0.00, $\frac{a}{2c}$), R = $\frac{2\pi}{a}$(0.50, $\frac{a}{2b}$, $\frac{a}{2c}$), T = $\frac{2\pi}{a}$(0.00, $\frac{a}{2b}$, $\frac{a}{2c}$), and Y = $\frac{2\pi}{a}$(0.00, $\frac{a}{2b}$, 0.00)

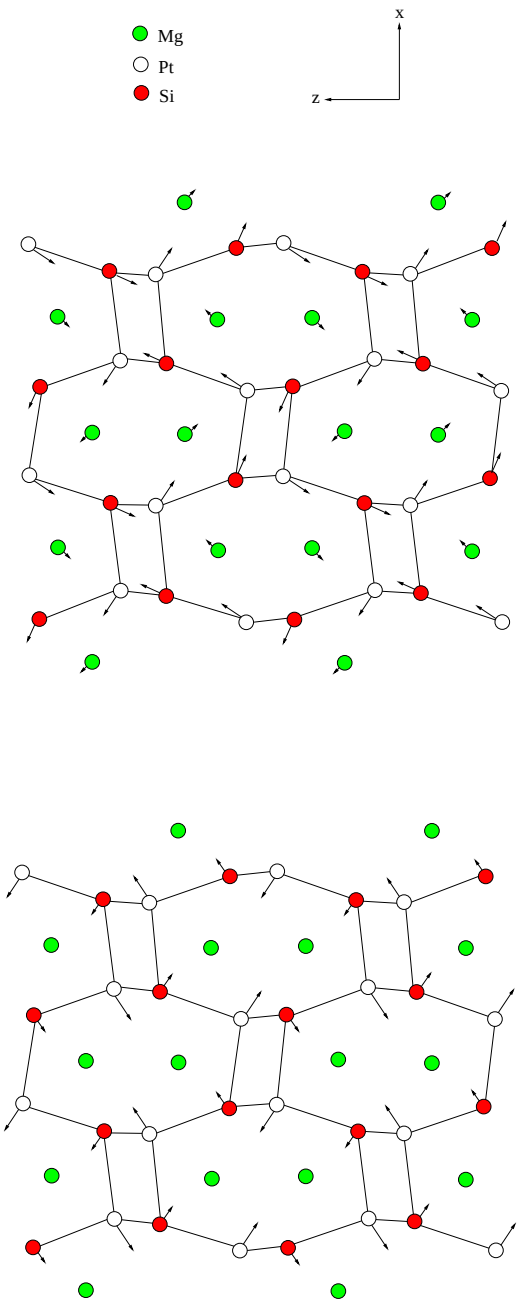

Fig. 3. The eigenvector representation of the first A_g mode (up panel) and the second A_g mode (down panel) in orthorhombic MgPtSi.

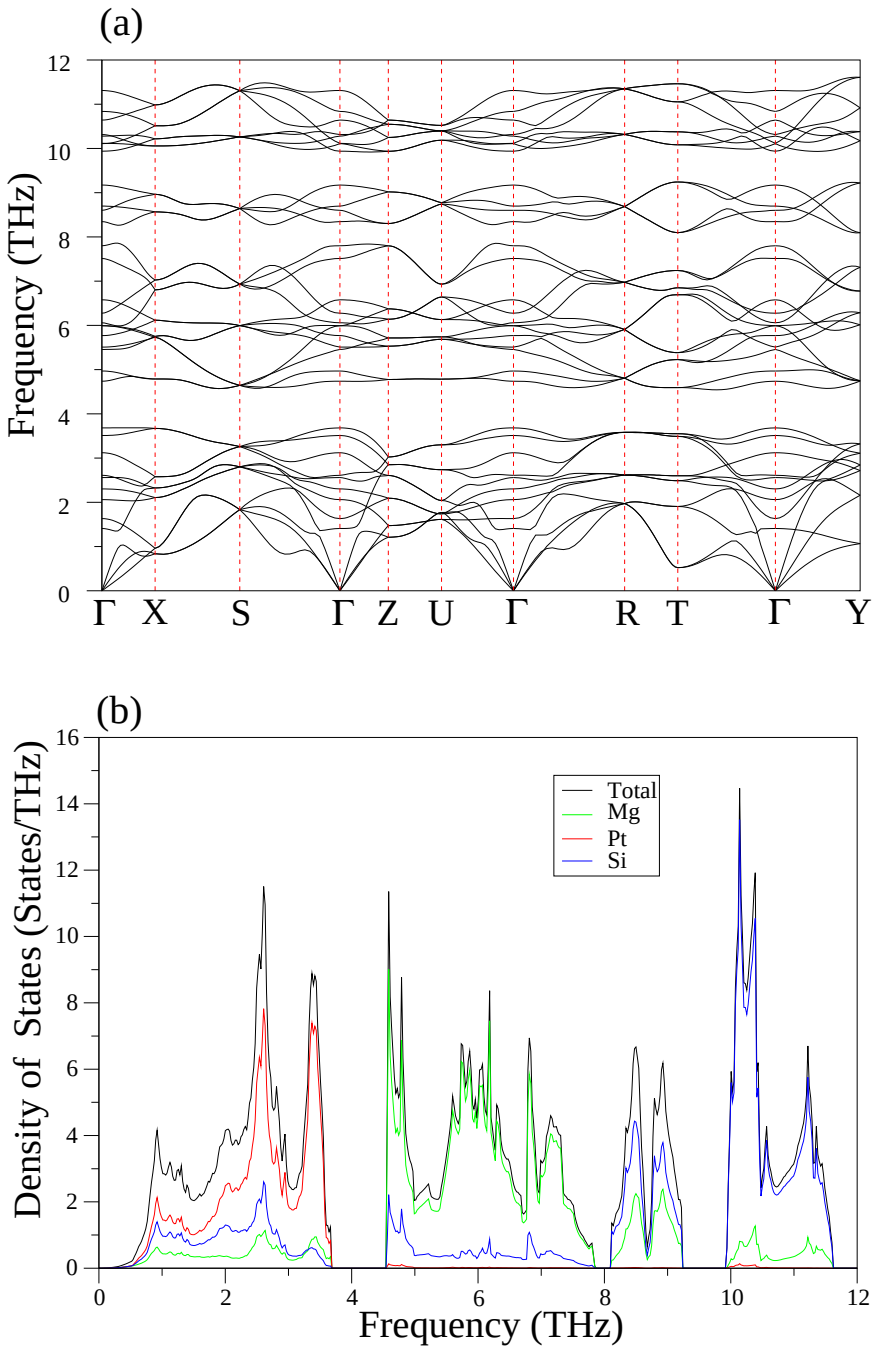

Fig. 4. (a) Calculated phonon spectrum for the orthorhombic MgPtSi along the symmetry lines of the simple orthorhombic Brillouin zone. (b) The calculated phonon total and atom-projected density of states for the orthorhombic MgPtSi.

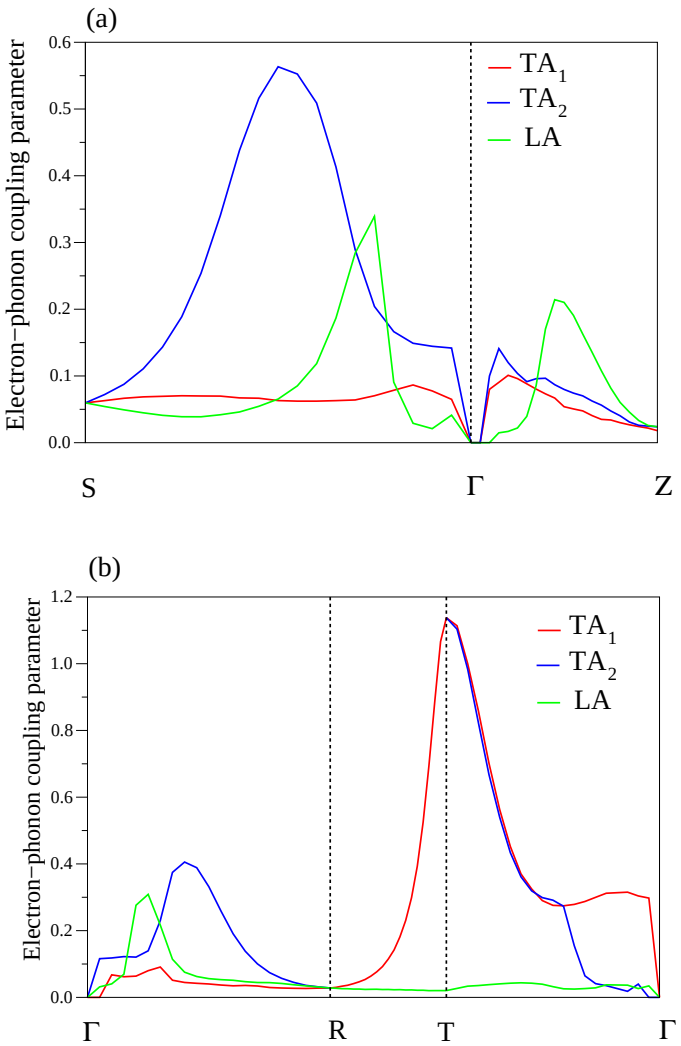

Fig. 5. The calculated wavevector-dependent electron-phonon coupling parameter for lower transverse acoustic branch (TA_1), upper transverse acoustic branch (TA_2) and longitudinal acoustic branch (LA) along the S-Γ-Z direction in MgPtSi. (b) The calculated wavevector-dependent electron-phonon coupling parameter for the TA_1, TA_2 and LA branches along the Γ-R-T-Γ direction in MgPtSi.

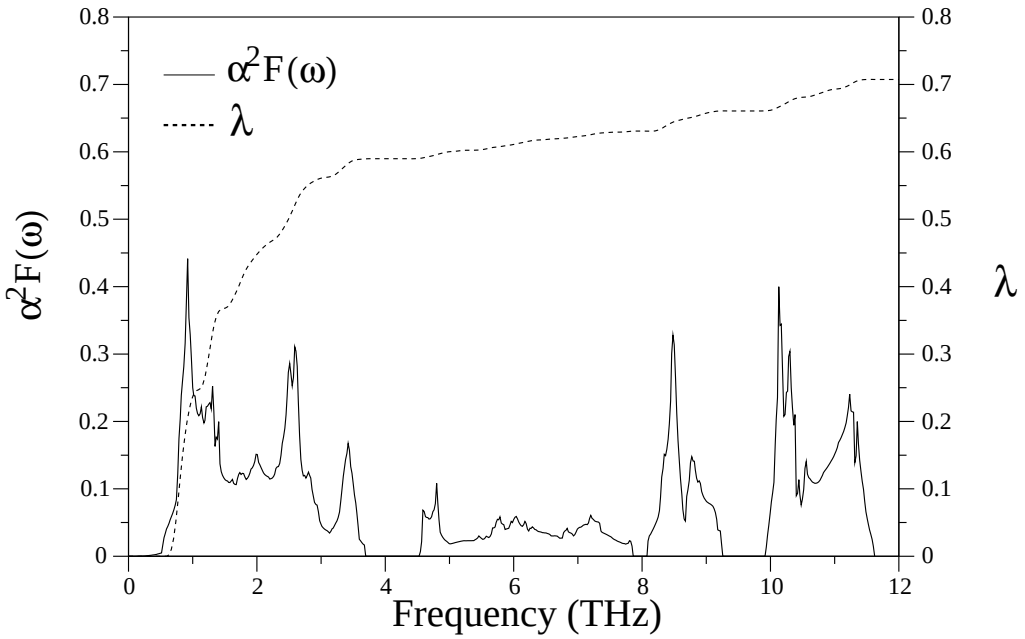

Fig. 6. The calculated electron-phonon spectral function $\alpha^2\mathrm{F}(\omega)$ (solid line) and the electron-phonon coupling parameter λ (dashed line) for MgPtSi.